Available online at www.sciencedirect.com
ScienceDirect
International Journal of Mass Spectrometry 255–256 (2006) 251–264
International Journal of Mass Spectrometry
www.elsevier.com/locate/ijms

Fragmentation of doubly charged metal–acetamide complexes: Second ionization energies and dissociation chemistries

Tujin Shi, K.W. Michael Siu *, Alan C. Hopkinson

Department of Chemistry and Centre for Research in Mass Spectrometry, York University, 4700 Keele Street, Toronto, Ont., Canada M3J 1P3

Received 13 December 2005; received in revised form 2 February 2006; accepted 6 February 2006
Available online 13 March 2006

In honor of Diethard Kurt Bohme, in recognition of his major contributions in the areas of mass spectrometry, gas-phase ion chemistry and thermochemistry.

Abstract

The dissociation chemistries of $[M(L)_n]^{2+}$ (M = Mg, Ca, Mn, Fe, Co, Ni, Cu, Zn; L = acetamide; n = 2–6) have been examined experimentally by tandem mass spectrometry and theoretically by density functional theory (DFT). At low collision energies, three primary reactions were observed: loss of acetamide to produce $[M(L)_{n-m}]^{2+}$; inter-ligand proton transfer followed by dissociation to form $[M(L-H)(L)_{n-2}]^+$ and protonated acetamide, $[L+H]^+$; and amide-bond cleavage, producing $[M(NH_2)(L)_{n-1}]^+$ and $[CH_3CO]^+$. Dissociative electron transfer from acetamide to the metal forming $[M(L)_{n-1}]^+$ and $[L]^{\bullet+}$ was only observed for $[Cu(L)_{2,3}]^{\bullet 2+}$ complexes. At higher collision energies, complexes containing deprotonated acetamide $[M(L-H)(L)_{n-2}]^+$ (except for $[Cu(L-H)(L)_{n-2}]^{\bullet+}$) further fragmented by eliminating small molecules (H_2O, CH_3CN, $H_2C{=}C{=}O$, HNCO) or by acetamide loss to produce $[M(L-H)]^+$; product ions $[M(NH_2)(L)_{n-1}]^+$ either eliminated ammonia to produce $[M(L-H)(L)_{n-2}]^+$ by inter-ligand proton transfer from one NH_2 group to another one, or lost acetamides to form $[M(NH_2)]^+$. Collision-induced dissociations of $[M(L-H)]^+$ yielded three common product ions, $[M(CH_3)]^+$, $[M(OH)]^+$, and M^+ by elimination of neutral molecules, HNCO, CH_3CN, and a neutral radical, $(L-H)^{\bullet}$, respectively. Elimination of methane from $[M(L-H)]^+$ was only observed for M = Ca, and elimination of the methyl group occurred for M = Co, Ni, and Zn. Copper complexes exhibited different chemistries; $[Cu(L-H)(L)]^{\bullet+}$ fragmented to either produce $[Cu(L)]^+$ by elimination of $(L-H)^{\bullet}$, or $[Cu(HNCO)(L)]^+$ by elimination of $CH_3^{\bullet}$; $[Cu(HNCO)(L)]^+$ further fragmented to produce $[Cu(L)]^+$ by elimination of HNCO. DFT calculations show that the gas-phase reactivities of $[M(L)_n]^{2+}$ complexes are closely related to the second ionization energies (IE2) of the metals. For the doubly charged $[M(L)_n]^{2+}$ species, as IE2 increases, fragmentations involving charge separation become more competitive: inter-ligand proton transfer becomes energetically more favorable than dissociation of a neutral ligand, and amide-bond cleavage occurs more readily. For singly charged ions $[M(L-H)L]^+$, for metals with low IE2 values, loss of L has a considerably lower enthalpy than loss of $(L-H)^{\bullet}$; however, for metals with higher IE2 values, loss of $(L-H)^{\bullet}$, which effectively reduces the oxidation state of the metal, becomes energetically competitive with the loss of L. The enthalpies for eliminating methane and the methyl radical from $[M(L-H)]^+$ (M = Ca, Mg, and Zn) have been calculated and correlate well with the experimental observations.

Keywords: Metal acetamide complexes; Dissociation; Electron transfer; Proton transfer; Second ionization energies

1. Introduction

One of the major differences between solution-phase and gas-phase chemistries is that the solvent stabilizes ions and hence promotes ionic reactions [1]. Investigation of gas-phase ion solvation provides a wealth of information on ion–solvent and ion–ligand interactions [2,3]. This knowledge is of importance not only to gas-phase ion chemistry, but also to the condensed phase, as ions solvated by a small number of solvent molecules constitute a bridge between the gas phase and solution [4–6]. With the development of ionization methods that can introduce solvated ions into a mass spectrometer and the application of high-level quantum chemical theory, ion–solvent binding can now be studied systematically [7–21].

Initial studies on metal–ligand complexes concentrated on singly charged metal ions, M^+ [2,3]. Work on doubly charged metal ions was limited to those that have low second ionization energies (IE2) [22] because of inherent charge reduction

* Corresponding author. Tel.: +1 416 650 8021; fax: +1 416 736 5936.
E-mail address: kwmsiu@yorku.ca (K.W.M. Siu).

1387-3806/$ – see front matter © 2006 Elsevier B.V. All rights reserved.
doi:10.1016/j.ijms.2006.02.004

associated with sequential ligation of M^{2+} by solvent molecules [6,23–25]. The IE of most common solvents are in the range of 8–13 eV (e.g., acetone, 9.7 eV; methanol, 10.8 eV; acetonitrile, 12.2 eV; and water, 12.6 eV), while the IE2 of most metals (with the exception of some alkaline-earth metals, Ba, 10.0 eV; Sr, 11.0 eV; and Ca, 11.9 eV) are above 13 eV [26]. Thus, electron transfer from a neutral ligand, L, to a doubly charged metal ion, M^{2+} is typically energetically favorable and should occur spontaneously, followed by the dissociation driven by Coulombic repulsion[1]:

$$[M(L)_n]^{2+} \rightarrow [M(L)_{n-1}]^{+} + L^{+} \quad (1)$$

If the ligand is a protic solvent, inter-ligand proton transfer can also take place readily, leading to formation of $[M(L-H)(L)_{n-2}]^{+}$, and the protonated ligand, $[L+H]^{+}$:

$$[M(L)_n]^{2+} \rightarrow [M(L-H)(L)_{n-2}]^{+} + [L+H]^{+} \quad (2)$$

These two channels are the only effective competitors to a third channel, ligand elimination for small *n*, when L is a simple ligand, e.g., H_2O [2,6,22,23,27–29].

$$[M(L)_n]^{2+} \rightarrow [M(L)_{n-1}]^{2+} + L \quad (3)$$

For ligands that are more complicated than water, other channels involving dissociative charge reduction, e.g., formation of the methyl cation, CH_3^{+}, have also been observed [30–33].

$$[M(CH_3CN)_n]^{2+} \rightarrow [M(CN)(CH_3CN)_{n-1}]^{+} + CH_3^{+}$$

and

$$[M(CH_3SOCH_3)_n]^{2+} \rightarrow [M(SOCH_3)(CH_3SOCH_3)_{n-1}]^{+} + CH_3^{+}$$

Metal–ligand complexes can be generated by electrospray ionization (ESI) and examined by mass spectrometry (MS). Since the early 1990s, ESI-MS has become the most frequently applied technique for the examination of gas-phase complexes of divalent metal cations with a variety of protic and aprotic ligands [7–13,29–47], including water [7–13,29,36–39,42–44], alcohols [39,40,45], acetone [8,39], other ketones [46], acetonitrile [30,39–41], pyridine [35,40], and dimethylsulfoxide (DMSO) [36,37,39,47]. Fragmentations of M^{2+}–ligand complexes, where the ligand is an aprotic solvent (CH_3CN, CH_3COCH_3 and DMSO), have been studied extensively. Complexes $[M(L)_n]^{2+}$ ($L = CH_3CN$, DMSO) where n is large, dissociate by loss of neutral ligands. As the number of ligands is decreased, there is competition between the electron transfer channel, forming $[M(L)_{n-1}]^{+}$ and L^{+} (reaction (1)), and inter-ligand proton transfer, forming $[M(L-H)(L)_{n-2}]^{+}$ and $([L+H]^{+}$ (reaction (2)). Heterolytic cleavage of the C–C bond yielding $[M(L-CH_3)]^{+}$ and CH_3^{+} is also observed in lower abundance [30]. For $[M(ROH)_n]^{2+}$ ($R = CH_3$, H), dissociative proton transfer is favored over dissociative electron transfer, leading to $[M(RO)(ROH)_{n-2}]^{+}$ in high abundance. Collisionally activated $[M(RO)(ROH)_{n-2}]^{+}$ further fragments to produce small ions, involving neutral loss and bond cleavage. For example, at low collision energies, complexes $[M(OH)(H_2O)]^{+}$ (M = Co, Mn, Ni) fragment either to give $[M(OH)]^{+}$ by loss of water, or to produce $[M(H_2O)]^{+}$ by loss of a neutral radical, $OH^{\bullet}$ [48].

In this study, we investigate the fragmentations of doubly charged metal–acetamide complexes in the gas phase. Acetamide (CH_3CONH_2) is a typical protic solvent; the first ionization energy is 9.65 ± 0.03 eV [26], lower than IE2 of all metals. It is an amide and is a good model for examining the interactions of metal ions with peptides, which simpler protic solvents, e.g., H_2O [7–13,29,36–39,42–44] and CH_3OH [39,40,45] cannot. Metal dication interaction with a ligand results in a drastic reorganization of the charge density; withdrawal of electron density from the ligand to the formally doubly charged metal ion results in weakening and activation of specific bonds of the ligand [49]. Thus, facile fragmentation of multiply charged metal–ligand complexes is often observed, and the dissociative processes that occur are frequently characteristic of a specific ligand or functional group [49].

Here, we report the fragmentation chemistries of $[M(L)_n]^{2+}$ (M = Mg, Ca, Mn, Fe, Co, Ni, Cu, Zn; L = acetamide), both in terms of tandem MS results and DFT calculations. In order to rationalize the reactivity, we systemically examine how the IE2 of metals affect the fragmentation pathways of $[M(L)_n]^{2+}$ and $[M(L-H)(L)_{n-2}]^{+}$. These results will provide a more detailed picture of reactivity patterns. Collision-induced dissociation (CID) of $[M(L)_n]^{2+}$ produces high abundances of $[M(L-H)]^{+}$ by inter-ligand proton transfer, followed by loss of protonated acetamide, $[L+H]^{+}$. The $[M(L-H)]^{+}$ ions can further fragment by eliminating small molecules. We also investigate the potential energy hypersurfaces (PESs) of competing fragmentation pathways, involving the elimination of a methane molecule or a methyl radical from $[M(L-H)]^{+}$, using density functional theory (DFT) calculations. The PESs results are compared and contrasted with our experimental observations.

2. Experimental section

Experiments were performed on MDS SCIEX (Concord, ON) API III and API 3000 prototype triple-quadrupole mass spectrometers. Samples were typically 1 mM acetamide and 0.1 mM divalent metal salts in 50/50 H_2O/CH_3OH. Confirmatory experiments were performed with solutions in propanamide. When needed, H/D exchange experiments were carried out in deuterium oxide (99.9 at.% in D, Aldrich) and CH_3OD (99.5 at.% in D, Aldrich) instead of H_2O and CH_3OH. The sample solution was introduced into the ion source by electrospraying at a flow rate of 3 μL/min. The orifice and lens voltages were optimized to produce abundant $[M(L)_n]^{2+}$ ions. All chemicals and solvents were available from Sigma/Aldrich (St. Louis, MO). MS/MS experiments were performed by mass-selecting the precursor ions using the first quadrupole mass analyzer (Q1), colliding them with argon (API III) and nitrogen

[1] In some of the complexes $[M(L)_n]^{2+}$, there are unpaired electrons while other complexes are closed shell ions. In order to generalize, we simply omit spins.

Table 1
Calculated ionization energies (IE, eV) of metals and acetamide at the B3LYP/6-311+G(d,p), compared with experiment results

Species	Calculation	Experiment [26]	Difference
IE(Mg)	7.73	7.65	+0.08
IE(Mg^+)	15.46	15.04	+0.42
IE(Ca)	6.15	6.11	+0.04
IE(Ca^+)	12.08	11.87	+0.21
IE(Cu)	8.04	7.72	+0.32
IE(Cu^+)	20.85	20.29	+0.56
IE(Zn)	9.43	9.39	+0.04
IE(Zn^+)	18.38	17.96	+0.42
IE(CH_3CONH_2)	9.87	9.65 ± 0.03	$+0.22 \pm 0.03$

(API 3000) in the second quadrupole (q2), and mass-analyzing with the third quadrupole (Q3). The laboratory collision energy (E_{lab}) was typically 10–50 eV.

3. Computational section

Geometry optimizations and energy calculations were performed with Gaussian'98 [50], using the B3LYP exchange-correlation functional [51–53] with the 6-311+G** triply split-valence basis set [54–57]. All stationary points were characterized by harmonic vibrational frequency calculations. All connections between transition states and corresponding minima were verified using the intrinsic reaction coordinate (IRC) method [58–59]. Relative enthalpies at 0 K (ΔH_0°) and relative free energies (ΔG_{298}°) at 298 K are reported.

To test the reliability of the B3LYP functional and the basis set, the ionization energies were calculated and compared to the available experimental data. Table 1 gives the first and second ionization energies of the metals, and the ionization energies of acetamide. All calculated energies are in reasonable agreement with measured energies. This indicates that the chosen level of theory is adequate for calculating the doubly charged M^{2+}–acetamide system.

4. Experimental results

4.1. Ion source condition

Electrospraying solutions of $M(NO_3)_2$ or MCl_2 with acetamide, L, produces abundant clusters of the types, $[M(L)_n]^{2+}$ and $[M(NO_3, Cl)(L)_m]^+$. The values of n and m depend on whether the ion sampling condition, the potential drop in the lens region, is "gentle" or "harsh". Under gentle source conditions (where the potential drop is small) typically n is 4–6, and m is 1–4. As the sampling conditions become harsher (the potential drop is larger), ligand elimination reduces the maximum value of n; charge reduction via inter-ligand proton transfer takes place in the source, leading to high abundances of $[M(L-H)(L)_{n-p}]^+$ and $[(L)_p+H]^+$. When exploring the dissociation of the $[M(L)_n]^{2+}$, it was expedient to fragment the smallest precursor ion that was present with a reasonably high abundance. For this reason, harsh conditions were sometimes adopted for tandem MS experiments.

4.2. Collision-induced dissociation (CID) of $[M(L)_n]^{2+}$ complexes

In addition to ligand elimination (reaction (3)), the $[M(L)_n]^{2+}$ complexes exhibited charge reduction by inter-ligand proton transfer (reaction (2)), and heterolytic cleavage of the amide bond (CO–NH_2):

$$[M(L)_n]^{2+} \rightarrow [M(NH_2)(L)_{n-1}]^+ + [CH_3CO]^+ \quad (4)$$

$[M(NH_2)(L)_{n-1}]^+$ can further dissociate to produce $[M(NH_2)]^+$ by losses of neutral ligands, or it can undergo inter-ligand proton transfer from an acetamide to the amino group to produce complexes $[M(L-H)(L)_{n-2}]^+$ with concomitant loss of ammonia. The $[M(L-H)(L)_{n-2}]^+$ complexes are also produced in reaction (2). The fragmentation of $[M(L-H)(L)_{n-2}]^+$ complexes provides us with the most useful insights into the factors influencing the dissociation of ions $[M(L)_n]^{2+}$.

4.3. Alkaline-earth metals: Ca, Mg

Of the metals examined, the alkaline-earth metals, Ca and Mg, have lower second ionization energies (IE2) than the transition metals. Complexes $[Ca(L)_n]^{2+}$ ($n \geq 3$) lose *only* neutral acetamide; no proton transfer or electron transfer was observed. In the CID of $[Ca(L)_2]^{2+}$, dissociative proton transfer (reaction (2)), giving $[Ca(L-H)]^+$ ($m/z = 98$) and protonated acetamide ($m/z = 60$) closely competes with acetamide elimination (reaction (3)), giving $[Ca(L)]^{2+}$ ($m/z = 49.5$) (Fig. 1a). As the collision energy increased, the products of amide-bond cleavage (reaction (4)), $[Ca(NH_2)]^+$ ($m/z = 56$) and $[CH_3CO]^+$ ($m/z = 43$), increased in abundance.[2] Another unusual feature, not observed for any other divalent metal ion–acetamide complex, was the loss of *both* acetamide molecules from $[Ca(L)]^{2+}$ to give bare Ca^{2+} ($m/z = 20$). The unusually abundant monoligated Ca^{2+} complex, $[Ca(L)]^+$, signifies that the complex is kinetically stable. In comparison, the CID of $[Ca(H_2O)_3]^{3+}$ produced very low abundance $[Ca(H_2O)]^{2+}$ and no Ca^{2+} [37]. At first glance, this may be puzzling in view of the facts that IE(H_2O) = 12.6 eV > IE2(Ca) = 11.87 eV > IE(acetamide) = 9.65 eV [26] (vide infra).

As discussed in Section 4.1, increasing the orifice voltage results in the fragmentation of doubly charged ions to produce abundant $[M(L-H)(L)_{n-2}]^+$ in the lens region. Fig. 1b gives the CID spectrum of $[Ca(L-H)]^+$ from the API III at a laboratory collision energy of 20 eV. Formation of both $[Ca(CH_3)]^+$

[2] At B3LYP/6-311+G** level, the amide bond dissociation enthalpy (ΔH_0°) for acetamide is 91.1 kcal/mol, 12.3 kcal/mol higher in energy than that of the H_3C—C bond (78.8 kcal/mol). By contrast, the dissociation enthalpy of the amide bond in $[Ca(L)]^{2+}$, giving $[Ca(NH_2)]^+$ and $[CH_3CO]^+$, is 6.3 kcal/mol, 25.2 kcal/mol lower in energy than that of the H_3C—C bond, giving $[Ca(CH_3)]^+$ and $[NH_2CO]^+$ (31.5 kcal/mol). Thus, the DFT calculations show that in $[Ca(L)]^{2+}$, the amide-bond cleavage is energetically more favorable than that of the H_3C—C bond, which is consistent with our experimental observation. These results are in accordance with the interpretation that the dication, Ca^{2+}, selectively activates the amide bond in $[Ca(L)]^{2+}$, resulting in the amide-bond cleavage.

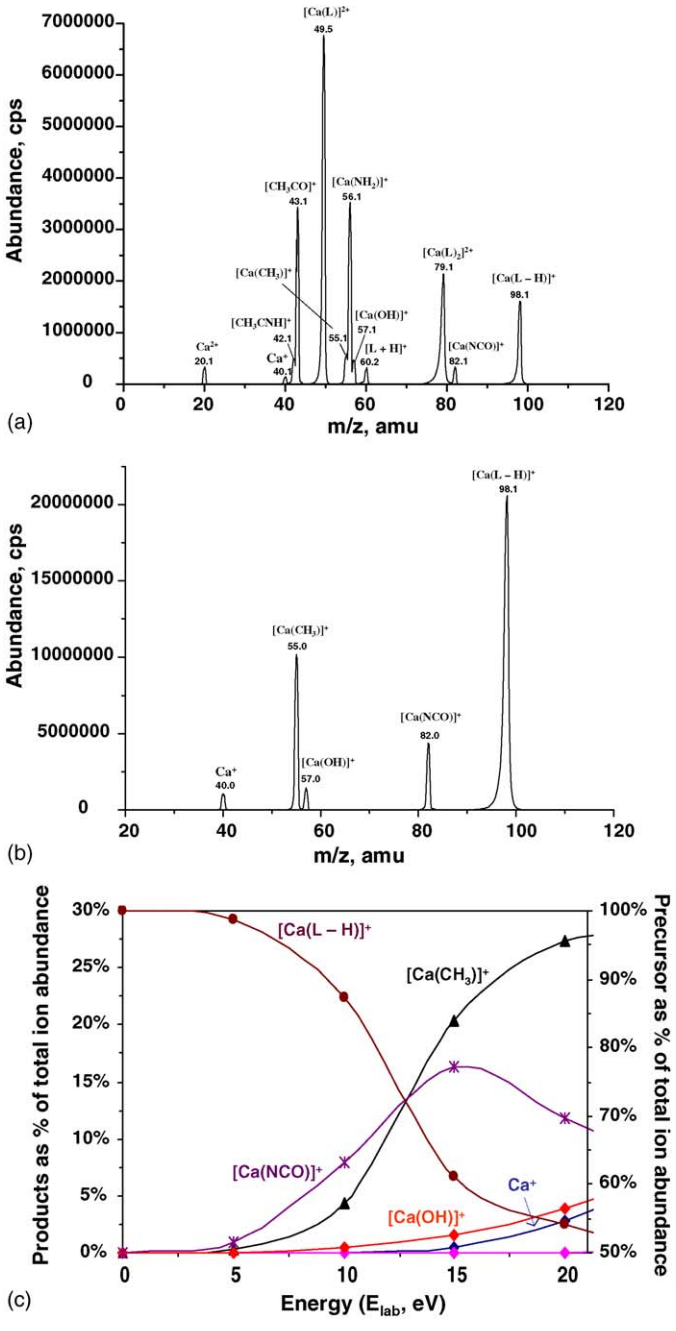

Fig. 1. CID spectra of (a) $[Ca(L)_2]^{2+}$ at $E_{lab} = 40$ eV, (b) $[Ca(L-H)]^+$ at $E_{lab} = 20$ eV on the API III under single-collision conditions with Ar, and (c) breakdown curves for $[Ca(L-H)]^+$ and product ions.

($m/z = 55$) and $[Ca(NCO)]^+$ ($m/z = 82$) requires C–C bond cleavage and these two products are most easily explained in terms of an intermediate $[(CH_3)Ca(HNCO)]^+$ complex, which may either lose HNCO, yielding $[Ca(CH_3)]^+$, or undergo a 1,3-proton shift to give $[Ca(NCO)]^+$ and CH_4. Energy-dependent CID data (Fig. 1c) show the latter process is favored at lower energies. These same two fragmentation pathways have also been observed in the fragmentation of $[Ca(urea-H)]^+$ [60].

At much higher collision energies, ion $[Ca(OH)]^+$ ($m/z = 57$) is formed. A possible mechanism for the formation of this ion involves a 1,3-proton shift from the NH of $[Ca(L-H)]^+$ to the oxygen, followed by cleavage of the C–O bond to give an intermediate complex, $[(HO)Ca(NCCH_3)]^+$, that eliminates CH_3CN; proton transfer between the incipient products[3] gives $[CH_3CNH]^+$ ($m/z = 42$), an ion that is in low abundance at high collision energies. It is noteworthy that the abundance of product ion $[CH_3CNH]^+$ from $[Ca(L)_2]^{2+}$ is much higher than that from $[Ca(L-H)]^+$, and that fragmentation of $[Ca(L)]^{2+}$ does not produce the combination of $[Ca(OH)]^+$ ($m/z = 57$) and $[CH_3CNH]^+$ ($m/z = 42$) by intra-ligand proton transfer. This suggests that, in the CID of $[Ca(L)_2]^{2+}$, the observed product ion, $[CH_3CNH]^+$, is formed directly from the precursor ion: Intra-ligand proton transfer from the amide nitrogen to the oxygen atom induces C–O bond cleavage and leads to the combination of $[CH_3CNH]^+$ ($m/z = 42$) and $[Ca(OH)(L)]^+$ ($m/z = 116$). Unfortunately, $[Ca(OH)(L)]^+$ was not observed in the CID spectrum of $[Ca(L)_2]^{2+}$, possibly due to its instability and/or the internal energy acquired from the charge separation reaction. The fragmentation pathways observed for $[Ca(L)_3]^{2+}$ are outlined in Scheme 1.

Dications of magnesium and calcium have the same outer electronic configurations as inert gases and might be expected to behave similarly. However, the IE2 of Mg (15.04 eV) is much higher than that of Ca (11.87 eV) [26], and generally, in collision-induced dissociations a higher IE2 favors charge reduction. Accordingly, the stability of $[Mg(L)_3]^{2+}$ is lower than that of $[Ca(L)_3]^{2+}$; the major dissociation channel of $[Ca(L)_3]^{2+}$ is loss of a ligand to form $[Ca(L)_2]^{2+}$, while for $[Mg(L)_3]^{2+}$, in addition to ligand loss, inter-ligand proton transfer results in dissociative proton transfer yielding $[Mg(L-H)(L)]^+$ ($m/z = 141$) and $[L+H]^+$ ($m/z = 60$) (Fig. 2a).

In a further illustration of the effect of a higher IE2, the fragmentation pattern of $[Mg(L)_2]^{2+}$ is substantially different from that of $[Ca(L)_2]^{2+}$. For $[Mg(L)_2]^{2+}$, amide-bond cleavage is the only operative reaction channel, producing singly charged ions $[Mg(NH_2)(L)]^+$ ($m/z = 99$) and $[CH_3CO]^+$ ($m/z = 43$); no inter-ligand proton transfer or ligand elimination was observed.

The CID spectrum of $[Mg(L-H)(L)]^+$ is shown in Fig. 2b at a laboratory collision energy of 20 eV. Loss of acetamide to give $[Mg(L-H)]^+$ ($m/z = 82$) is the dominant channel. Formation of ions $[Mg(CH_3CN)(L-H)]^+$ ($m/z = 123$) and $[Mg(H_2O)(L-H)]^+$ ($m/z = 100$) in low abundance are most easily rationalized by proton shifts from the NH_2 of the neutral ligand to the carbonyl oxygen, as outlined in Scheme 2. Density functional theory calculations (Scheme 3) at B3LYP/6-311+G(d,p) showed (L – H), essentially an acetylamino anion, is di-coordinated through both the oxygen and nitrogen to Mg^{2+}, while the acetamide ligand, L, is mono-coordinated through the oxygen. Intra-ligand migration of one amide hydrogen in L to the carbonyl oxygen has a barrier of 54.1 kcal/mol and creates a hydroxylimine coordinated to the Mg^{2+} through the oxygen. The complex in which the hydroxylimine is coordinated through the imine nitrogen has a lower energy (by 19.3 kcal/mol) and rear-

[3] Proton affinity (PA) of CaO = 284.6 kcal/mol > PA of CH_3CN = 186.2 kcal/mol [61].

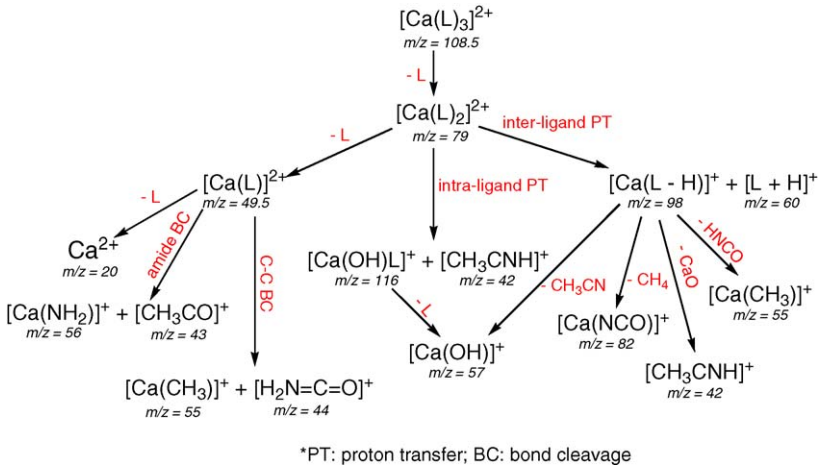

Scheme 1.

rangement of this ion via a transition state in which a proton is migrating from the imino nitrogen concomitant with C–O bond cleavage results in 4-coordinated Mg^{2+} in which water and acetonitrile are both ligands. This latter structure lies only 4.7 kcal/mol above $[Mg(L-H)(L)]^+$ and the barrier against its formation is 76.9 kcal/mol. Loss of H_2O or CH_3CN from this 4-coordinate complex has a comparatively low barrier (33.3 or 45.3 kcal/mol) than that against the formation of the complex, and should, therefore, occur spontaneously.

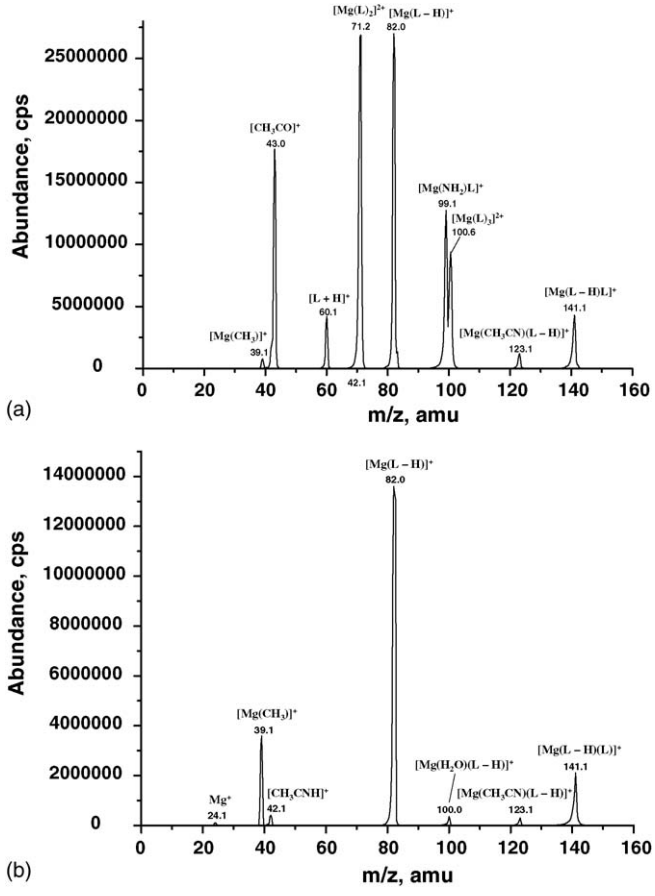

Fig. 2. CID of (a) $[Mg(L)_3]^{2+}$ at $E_{lab} = 40$ eV, and (b) $[Mg(L-H)(L)]^+$ at $E_{lab} = 20$ eV on the API III under single-collision conditions with Ar.

Elimination of HNCO from $[Mg(L-H)]^+$ results in formation of $[Mg(CH_3)]^+$ ($m/z = 39$), an analogous reaction to that observed for $[Ca(L-H)]^+$; however, in contrast to the calcium complex, the formation of $[Mg(NCO)]^+$ was not observed. In the CID of $[Mg(L-H)]^+$, C–O bond cleavage produced abundant $[CH_3CNH]^+$ ($m/z = 42$) with concomitant loss of MgO[4]. Formation of $[MgOH]^+$ ($m/z = 41$) requires a 1,3-proton transfer from the incipient $[CH_3CNH]^+$ to the incipient MgO. The overall fragmentation pathways exhibited by $[Mg(L)_3]^{2+}$ are summarized in Scheme 3.

4.4. Transition metals: Mn, Fe, Co, Ni and Zn

CID spectra of $[M(L)_3]^{2+}$ (M = Mn, Fe, Co, Ni, Zn) as recorded on the API III at laboratory collision energies of 40 eV were all very similar; by way of illustration, the spectrum for $[Co(L)_3]^{2+}$ is shown in Fig. 3. The relative abundances of the product ions for all the $[M(L)_3]^{2+}$ complexes are given in Table 2. CID of these complexes (Scheme 4) displays again two major fragmentation pathways, loss of a neutral ligand to form $[M(L)_2]^{2+}$ and inter-ligand proton transfer accompanied by dissociation to produce two singly charged ions, $[M(L-H)(L)]^+$ and $[L+H]^+$. As discussed earlier, the second pathway involves charge reduction and is expected to be favored for complexes of metals that have high IE2 values. Again, ions $[M(L-H)(L)]^+$ lose ligand L, to give $[M(L-H)]^+$, and these ions have the highest abundance in half the spectral results reported in Table 2.

Three low abundance ions $[M(CH_3)]^+$, $[M(NH_2)]^+$ and $[M(OH)]^+$ were observed in the CID of $[M(L)_3]^{2+}$. Ions $[M(NH_2)]^+$, where M is Mn, Fe and Co, most likely originate from loss of L from $[M(NH_2)L]^+$; however, when M is

[4] As alluded to earlier, the equivalent reaction is not favored in the CID of $[Ca(L-H)]^+$; the difference may lie in the relatively low PA of MgO (236 kcal/mol) [61].

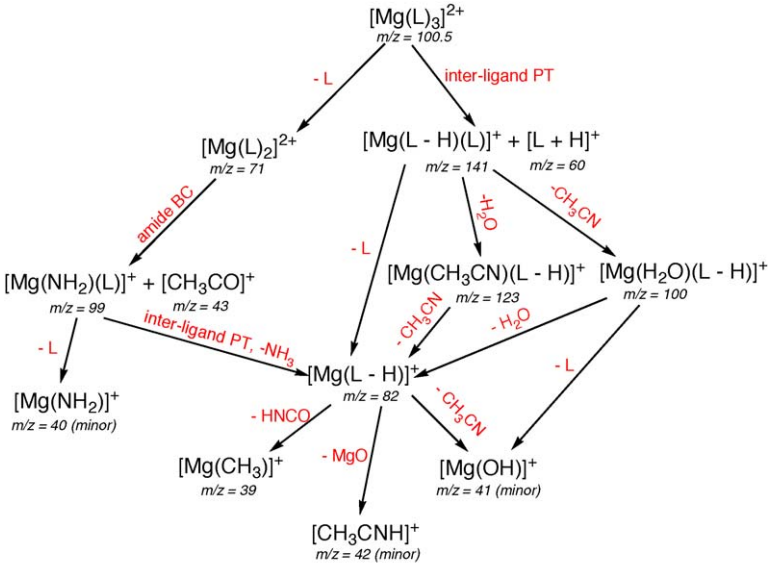

Scheme 2.

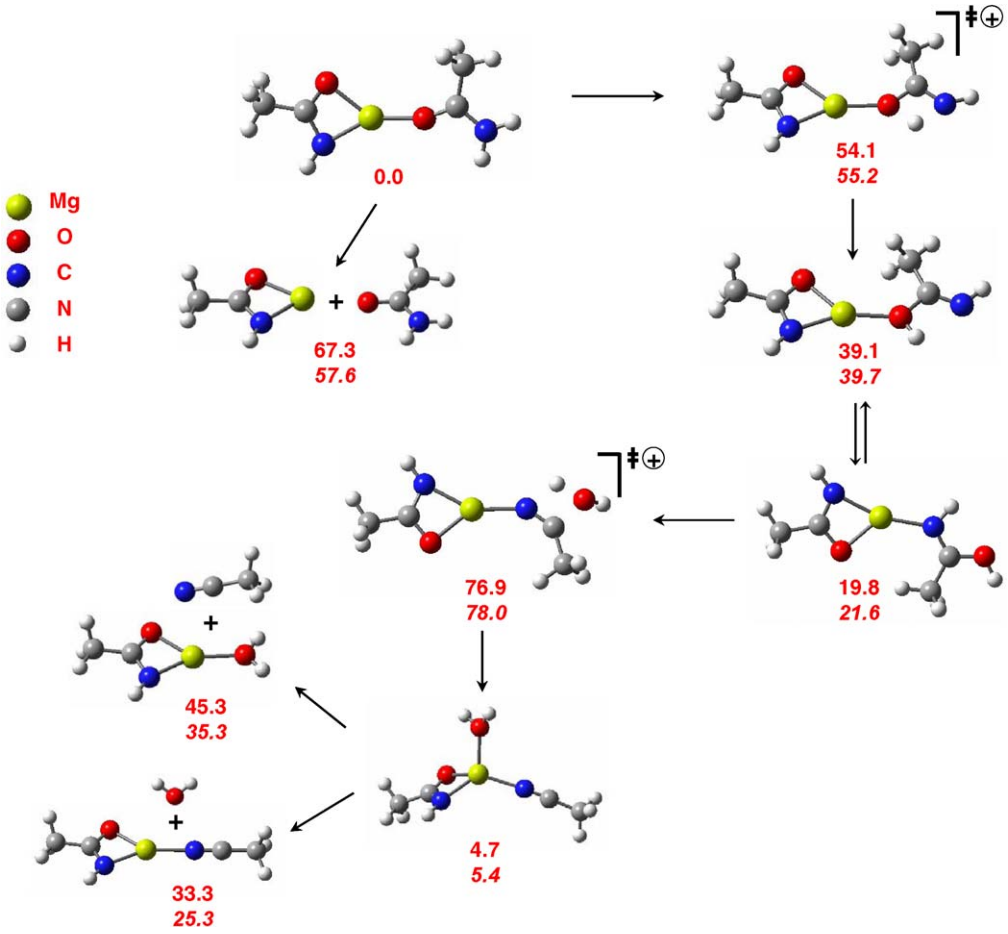

Scheme 3.

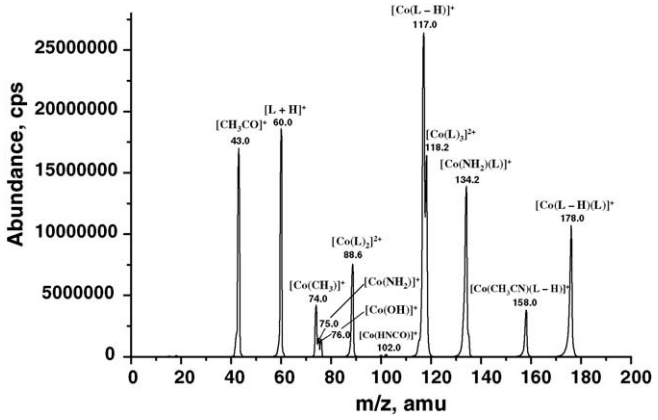

Fig. 3. CID spectrum of $[Co(L)_3]^{2+}$ at $E_{lab} = 40$ eV on the API III under single-collision conditions with Ar.

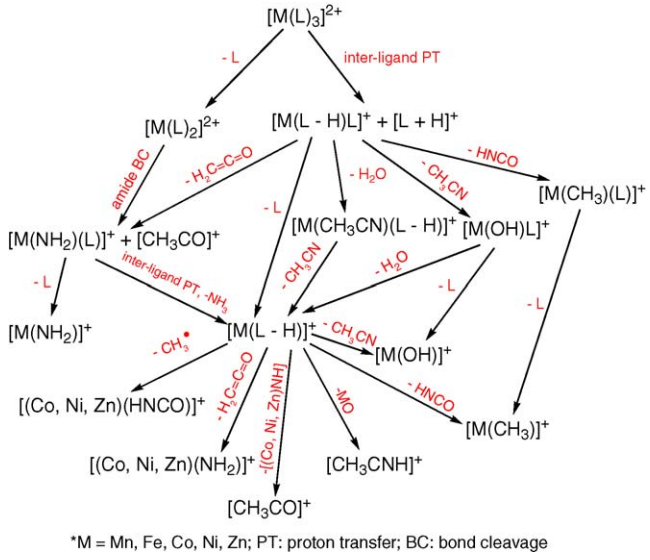

Scheme 4.

Ni and Zn, an additional source may be from $[M(L-H)]^+$ by loss of $H_2C{=}C{=}O$, involving intra-ligand proton transfer from the methyl group to the imino group accompanied by cleavage of the C–N bond.

As in $[Mg(L)_2]^{2+}$, loss of a ligand from $[M(L)_2]^{2+}$ to give $[M(L)]^{2+}$ was not observed. Instead, ions $[M(L)_2]^{2+}$ undergo charge separation reactions to yield two singly charged ions, $[CH_3CO]^+$ and $[M(NH_2)(L)]^+$. Elimination of ammonia from the latter ion gives $[M(L-H)]^+$; and loss of the neutral ligand from $[M(NH_2)(L)]^+$ produces the $[M(NH_2)]^+$ ion. DFT calculations show that $[Mg(NH_3)(L-H)]^+$ is lower than $[Mg(NH_2)(L)]^+$ in terms of enthalpy at 0 K by 20.7 kcal/mol, and conversion from the latter to the former has a very low barrier ($\Delta H_0^{\ddagger}$) of 7.7 kcal/mol.

The primary dissociation channel of $[M(L-H)L]^+$ is again the elimination of acetamide to yield $[M(L-H)]^+$. At low collision energies, several other dissociation channels were observed: elimination of H_2O from $[M(L-H)L]^+$ yields $[M(CH_3CN)(L-H)]^+$, involving two sequential hydrogen transfers and probably following similar pathways as shown for $[Mg(L-H)(L)]^+$ in Scheme 3; elimination of HNCO, $H_2C{=}C{=}O$ and CH_3CN from $[M(L-H)L]^+$ resulting in the formation of $[M(CH_3)L]^+$, $[M(NH_2)L]^+$, and $[M(OH)L]^+$, respectively. These minor products can further fragment to give $[M(L-H)]^+$, with concomitant losses of the complementary neutral parts, or to produce small product ions, $[M(CH_3)]^+$, $[M(NH_2)]^+$ and $[M(OH)]^+$, respectively. The $[M(X)L]^+$ and $[M(X+H)(L-H)]^+$ ions (X = CH_3, NH_2 and OH) are similar in energies and are separated by relatively small barriers. For M = Mg and Zn, the ΔH_0° of $[M(X+H)(L-H)]^+$ ions and the conversion barrier from $[M(X)L]^+$ ions are, respectively: X = NH_2, M = Mg, −20.7 and 7.7 kcal/mol (see above), M = Zn, −9.9 and 17.7 kcal/mol; X = OH, M = Mg, −0.3 and 17.9 kcal/mol, M = Zn, 7.2 and 28.1 kcal/mol; and X = CH_3, M = Mg, 0.8 and 37.6 kcal/mol, M = Zn, 28.6 and 60.6 kcal/mol. $[M(CH_3CN)]^+$ ions were only observed in the CID spectra of ions with M = Ni and Zn.

Details of the CID spectra of the $[M(L-H)]^+$ ions (M = Mn, Fe, Co, Ni, Zn) at $E_{lab} = 20$ eV are shown in Table 3 and one representative spectrum, that of $[Co(L-H)]^+$, is given in Fig. 4. Three common products, $[M]^+$, $[M(CH_3)]^+$ and $[M(OH)]^+$ were observed, corresponding to eliminations of $[L-H]^{\bullet}$, HNCO and CH_3CN, respectively. Loss of HNCO requires breaking the C–C bond, as does loss of $CH_3^{\bullet}$; retention of HNCO as the ligand and loss of $CH_3^{\bullet}$ was observed in the CID of $[M(L-H)]^+$ complexes of metals that have the higher IE2 values (Co, 17.06 eV; Zn 17.96 eV; and Ni, 18.17 eV). Furthermore, there appears to be correlation with IE2, as the abundance was highest for $[Ni(HNCO)]^+$.

Table 2
Ions in the CID spectra of $[M(L)_3]^{2+}$ (L = acetamide) at $E_{lab} = 40$ eV, under single-collision conditions

M	$[M(L)_3]^{2+}$	$[M(L-H)(L)]^+$	$[M(NH_2)(L)]^+$	$[M(L-H)]^+$	$[M(L)_2]^{2+}$	$[L+H]^+$	$[CH_3CO]^+$
Mg	34	17	47	100	100	17	65
Ca	16	0.5	2	54	100	13	19
Mn	19	10	40	100	48	25	50
Fe	18	14	46	100	25	65	69
Co[a]	60	41	52	100	28	69	63
Ni	41	32	48	88	41	100	37
Cu[b]	41	12	25	n/a	20	28	40
Zn	42	50	82	94	11	68	100

[a] $[Co(CH_3)]^+$, 16%; $[Co(CH_3CN)(L-H)]^+$, 16%.
[b] $[Cu(L)]^+$, 100%; $[L]^{\bullet+}$, 26%.

Table 3
Ions in the CID spectra of $[M(L-H)]^+$ (L = acetamide) at E_{lab} = 20 eV, under single-collision conditions

M	$[M(L-H)]^+$	$[M(HNCO)]^+$	$[M(OH)]^+$	$[M(NH_2)]^+$	$[M(CH_3)]^+$	$[M]^+$	$[CH_3CNH]^+$	Other
Mg	100	n/a	n/a	n/a	27	1	3	
Ca	100	n/a	5	n/a	48	4	n/a	$[Ca(NCO)]^+$, 22
Mn	100	n/a	60	n/a	20	15	11	
Fe	100	n/a	58	n/a	33	8	16	
Co	100	3	30	n/a	35	12	21	
Ni	100	49	4	16	13	30	1	
Cu	n/a	n/a	n/a	n/a	n/a	n/a	n/a	
Zn	100	32	21	6	12	28	n/a	$[Zn(CH_3CN)]^+$, 4

As discussed earlier for the Ca complex, formation of $[M(OH)]^+$ from $[M(L-H)]^+$ involves hydrogen migration from the imino group to the oxygen atom, followed by C–O bond cleavage and loss of CH_3CN. Mechanistically, this occurs most easily if the (L – H) is mono-coordinated through the oxygen atom. For $[Mn(L-H)]^+$, the complex containing the transition metal with the lowest IE2, and one in which mono-coordination is therefore probably most easily achieved, this is the dominant pathway. Interestingly, as IE2 of the metal increases, cleavage of the C–C bond leading to loss of $CH_3^\bullet$ or HNCO, a reaction that can occur from the di-coordinated complex, becomes the preferred pathway. Here, it should be noted that the *final* products of this latter type of cleavage are both mono-coordinate.

Energy-dependent data for the dissociation of $[Zn(L-H)]^+$ are given in Fig. 5. Formation of $[Zn(HNCO)]^+$, $[Zn(CH_3)]^+$ and $[Zn(OH)]^+$ all start at similar energies, while formation of $[Zn(NH_2)]^+$ and Zn^+ requires higher energies. Formation of $[M(NH_2)]^+$, observed only in the CID of complexes of the metals with the highest IE2 values (Ni and Zn), requires hydrogen migration from the methyl group of $[M(L-H)]^+$ to the imino group, followed by elimination of $CH_2{=}C{=}O$.

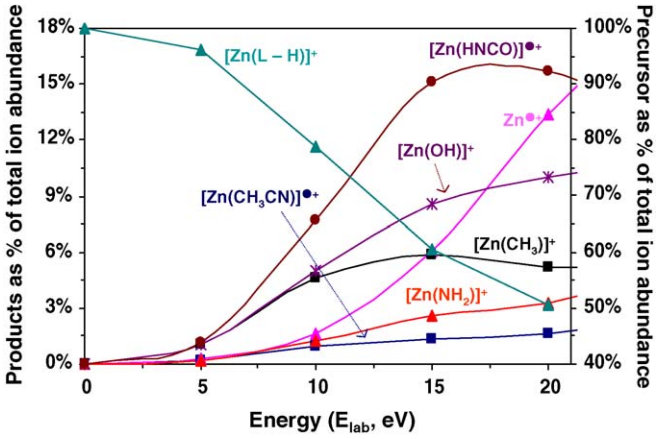

Fig. 5. Breakdown curves for $[Zn(L-H)]^+$ and product ions.

4.5. Copper

Copper has the highest IE2 (20.3 eV) of all transition metals; CID of its $[Cu(L)_n]^{\bullet 2+}$ complexes display different types of fragmentation pathways from the complexes of the dications of other transition metals. In particular, charge-reduction pathways are more prevalent. Fig. 6a and b show the CID spectra of $[^{65}Cu(L)_4]^{2+}$ and $[^{65}Cu(L)_3]^{2+}$ at laboratory collision energies of 40 eV, respectively. The MS/MS spectra for the analogous ions of the copper isotope, ^{63}Cu, were used as aids to make definitive identifications of all copper-containing ions. A summary of the overall fragmentation pathways observed for $[Cu(L)_3]^{\bullet 2+}$ and its product ions is shown in Scheme 5.

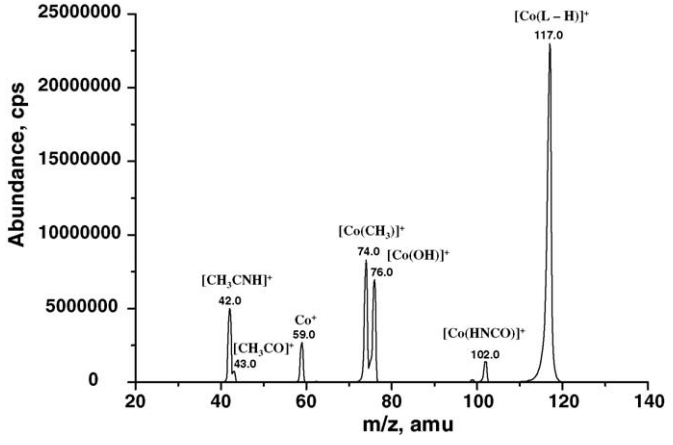

Fig. 4. CID spectrum of $[Co(L-H)]^+$ at E_{lab} = 20 eV on the API III under single-collision conditions with Ar.

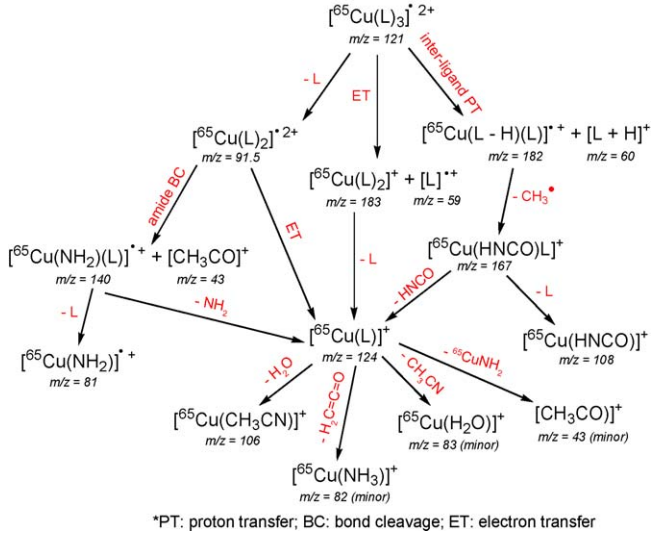

Scheme 5.

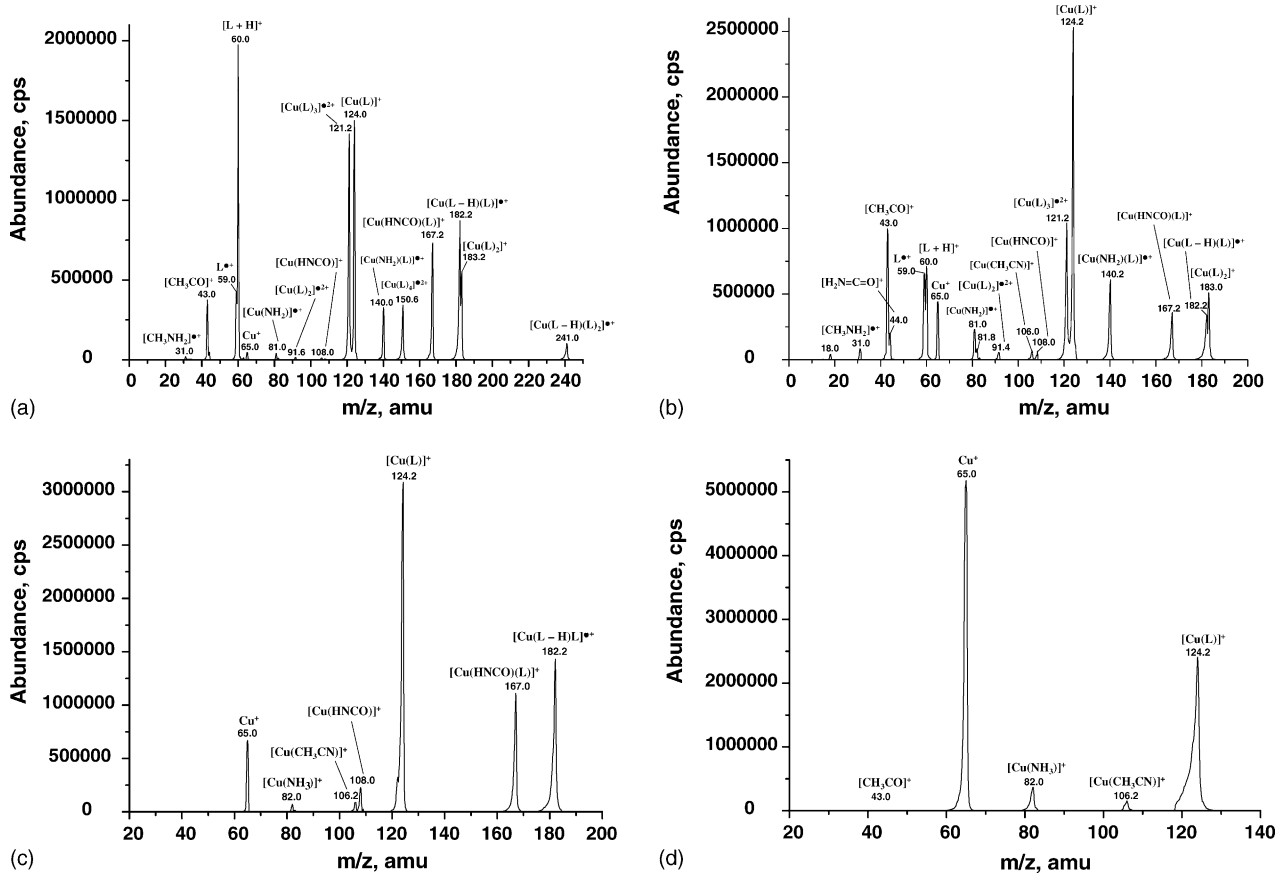

Fig. 6. CID spectra of (a) $[^{65}Cu(L)_4]^{\bullet 2+}$ (E_{lab} = 40 eV), (b) $[^{65}Cu(L)_3]^{\bullet 2+}$ (E_{lab} = 40 eV), (c) $[^{65}Cu(L-H)L]^{+}$ (E_{lab} = 20 eV), and (d) $[^{65}Cu(L)]^{+}$ (E_{lab} = 30eV) on the API III under single-collision conditions with Ar.

Collision-induced dissociation of $[^{65}Cu(L)_4]^{\bullet 2+}$ (m/z = 150.5) results in either loss of acetamide to give $[^{65}Cu(L)_3]^{\bullet 2+}$ (m/z = 121.0), or charge reduction by inter-ligand proton transfer accompanied by dissociation to give $[^{65}Cu(L-H)(L)_2]^{\bullet 2+}$ (m/z = 241.0) and $[L+H]^+$. At all collision energies, loss of the neutral ligand was the dominant channel. No $[Cu(L)_3]^+$ (m/z = 242.0) was observed, indicating that charge reduction by electron transfer from a ligand molecule to the metal ion, followed by dissociation did not occur.

In the CID of $[^{65}Cu(L)_3]^{\bullet 2+}$, loss of a neutral ligand to produce $[^{65}Cu(L)_2]^{\bullet 2+}$ (m/z = 91.5) is a minor channel (Fig. 6b) and charge-reduction pathways predominate. The products of dissociative proton transfer ($[^{65}Cu\ (L-H)(L)]^{\bullet +}$ (m/z = 182.0) and $[L+H]^+$) are in slightly higher abundance than those of the electron transfer reaction ($[Cu(L)_2]^+$ (m/z = 183.0) and $[L]^{\bullet +}$ (m/z = 59.0). Ions $[M(L)_2]^+$, the product of this last pathway, were not detected in the CID spectra of *any* of the other $[M(L)_3]^{2+}$ complexes examined here. However, this type of reaction is common in the complexes of doubly/triply charged metal ions containing aprotic solvents, such as DMSO [33,47], and acetonitrile [30], but is less prominent for protic solvent complexes [29,40].

At higher orifice voltages, charge reduction reactions (proton transfer and electron transfer) produce singly charged species in the lens region. The CID spectrum of $[^{65}Cu(L-H)(L)]^{\bullet +}$ (m/z = 182) at laboratory collision energy of 20 eV is shown in Fig. 6c. Similar to the CID of $[^{58}Ni(L-H)]^+$, two primary dissociation channels were observed: loss of the methyl radical, yielding $[^{65}Cu(HNCO)(L)]^+$ (m/z = 167); and elimination of the neutral $(L-H)^{\bullet}$, resulting in formation of abundant $[^{65}Cu(L)]^+$ (m/z = 124). No acetamide elimination was observed from $[^{65}Cu(L-H)(L)]^+$. As the collision energy increased, the product ion $[Cu(HNCO)(L)]^+$ further eliminated either HNCO to produce $[^{65}Cu(L)]^+$ (m/z = 124) or acetamide to give $[^{65}Cu(HNCO)]^+$ (m/z = 108).

In the CID of $[^{65}Cu(L)_2]^+$ (m/z = 183), the dominant channel is the loss of acetamide, yielding $[^{65}Cu(L)]^+$ (m/z = 124). The CID spectrum of $[^{65}Cu(L)]^+$ (Fig. 6d) shows several products resulting from different dissociation pathways. The major channel corresponds to elimination of the neutral ligand to produce $^{65}Cu^+$. Ions of low abundance, $[Cu(CH_3CN)]^+$ (m/z = 106) and $[Cu(NH_3)]^+$ (m/z = 82), are formed via eliminations of H_2O and $H_2C{=}C{=}O$, respectively. The minor product $[CH_3CO]^+$ (m/z = 43) probably comes from either proton transfer from $[Cu(NH_3)]^+$ to ketene, or elimination of $^{65}Cu(NH_2)$ from $[^{65}Cu(L)]^+$.

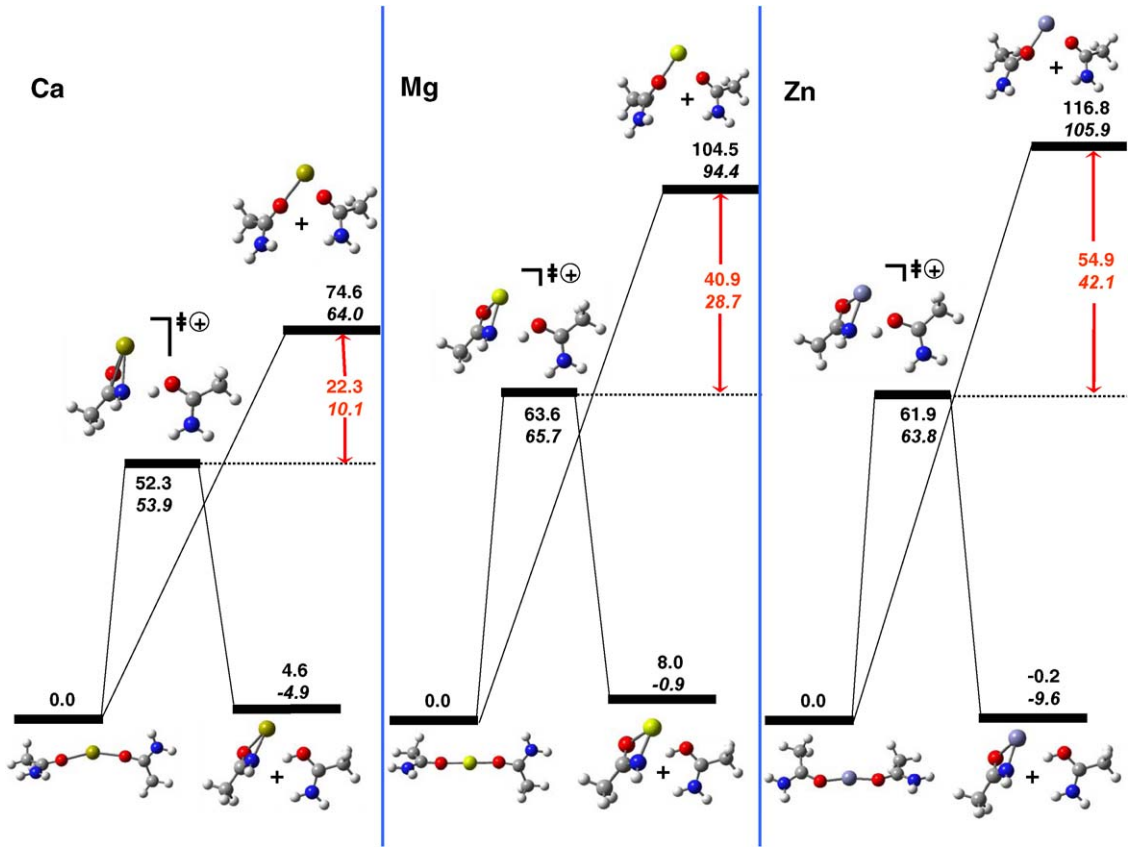

Fig. 7. Potential energy hypersurfaces for inter-ligand proton transfer and elimination of acetamide from $[M(L)_2]^{2+}$ complexes, where M = Ca, Mg, Zn: upper numbers are ΔH_0° and italicized lower number are ΔG_{298}°; both values are in kcal/mol.

5. Systemic theoretical studies

5.1. Charge reduction versus the second ionization energies (IE2)

5.1.1. Inter-ligand proton transfer

Collision-induced dissociations of $[M(L)_n]^{2+}$ complexes result in loss of a neutral ligand, when n is large (reaction (3)). However, when $n \leq 3$, charge reduction becomes important, inter-ligand proton transfer accompanied by dissociation (reaction (2)) to produce $[M(L-H)(L)]^+$ and $[L+H]^+$ competes with ligand elimination. In the special case of $[Cu(L)_3]^{\bullet 2+}$, a second charge-reduction channel, dissociative electron transfer giving $[Cu(L)_2]^+$ and $L^{\bullet +}$ (reaction (1)), occurs. These phenomena parallel those observed in $[Cu(H_2O)_n]^{2+}$ [6,29,37]. In order to compare the energetics of the ligand loss and dissociative proton transfer channels, we have chosen to examine reaction profiles for the fragmentation of $[M(L)_2]^{2+}$, where M = Ca, Mg and Zn (Fig. 7).

In the $[M(L)_2]^{2+}$ complexes, both acetamides are singly coordinated to the metal through oxygen atoms. In the transition states for proton transfer, one ligand is essentially detached from the metal, a proton is migrating from the amide group of the other acetamide, forming an amide anion, and this anionic nitrogen is becoming coordinated to the metal. The dissociative proton-transfer barriers ($\Delta H_0^{\ddagger}$) for $[M(L)_2]^{2+}$ are Ca, 52.3 kcal/mol; Mg, 63.6 kcal/mol; and Zn, 61.9 kcal/mol. These are 22.3, 40.9 and 54.9 kcal/mol lower than the corresponding dissociation energies for neutral ligand loss. From this limited set of data, we note that the energy difference between the proton transfer barrier and the dissociation energy for neutral loss correlates with the IE2 (see Fig. 8). As the ionization energy increases, the energy differences, $\Delta\Delta H_0^\circ$ and $\Delta\Delta G_{298}^\circ$, become larger, which means that inter-ligand proton transfer is increasingly more favorable relative to the loss of acetamide.

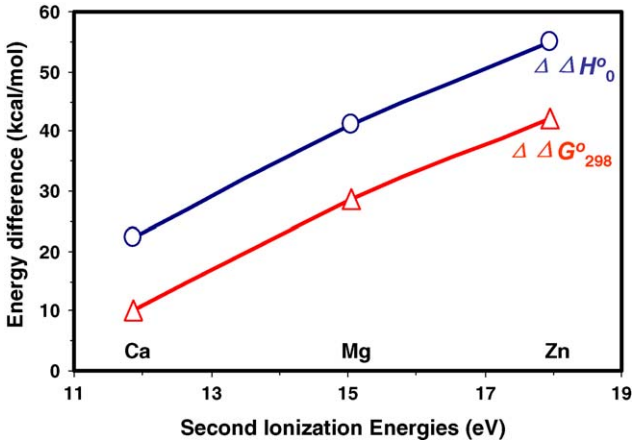

Fig. 8. Energy differences ($\Delta\Delta H_0^\circ$, $\Delta\Delta H_{298}^\circ$) between the activation barriers against proton transfer and the dissociation energies of acetamide loss for $[M(L)_2]^{2+}$, M = Ca, Mg and Zn; both values are kcal/mol.

The dissociative proton-transfer barrier of 52.3 kcal/mol for $[Ca(L)_2]^{2+}$ is considerably higher than that of 33.3 kcal/mol for $[Ca(H_2O)]^{2+}$ [62]. The higher barrier is probably due to a relatively lower acidity of the amide hydrogen in the acetamide complex versus the hydroxide hydrogen in the water complex. In the lowest energy structure of $[Ca(L)_2]^{2+}$, the amide hydrogen is attached to an atom that is γ to Ca^{2+}, whereas in $[Ca(H_2O)]^{2+}$, the hydroxide hydrogen is attached to an atom that is α to Ca^{2+}. Indeed, proton transfer in $[Ca(L)_2]^{2+}$ is concurrent with coordination of Ca^{2+} by the amide nitrogen, which increases the acidity of the amide hydrogens due to polarization by the doubly charged calcium ion.

5.1.2. Amide-bond cleavage

A second charge reduction reaction in the CID of $[M(L)_n]^{2+}$, involving amide-bond cleavage, produces ions $[M(NH_2)(L)_{n-1}]^+$ and $[CH_3CO]^+$. Our experimental results show that as IE2 increases, the amide-bond cleavage channel becomes more prominent. For example, the IE2 of Ca is 11.67 eV, 3.17 eV lower than that of Mg at 15.04 eV [26]; $[Ca(L)_2]^{2+}$ dissociates to produce $[Ca(L)]^{2+}$ by loss of a neutral ligand, and no amide-bond cleavage was observed; by comparison, $[Mg(L)_2]^{2+}$ fragments to yield the singly charged $[Mg(NH_2)L]^+$ by amide-bond cleavage.

To model the dissociation of the C–N bond, we have chosen to examine ions $[M(L)]^{2+}$, where M = Ca, Mg, Zn, Ni, and Cu:

$$[M(L)]^{2+} \rightarrow [M(NH_2)]^+ + [CH_3CO]^+$$

Fig. 9 shows the potential energy hypersurface of $[Zn(L)]^{2+}$ as a general illustration. Migration of Zn^{2+} towards the nitrogen results in **IM1**, in which the metal ion is di-coordinated by the oxygen and nitrogen atoms. Cleavage of the Zn–O bond and elongation of the C–N bond results in $[Zn(NH_2)]^+$ and $[CH_3CO]^+$. The forward barrier of the dissociation reaction, $\Delta H_0^{\ddagger}$, is represented by **TS2**, which sits at 19.2 kcal/mol. The products $[Zn(NH_2)]^+$ and $[CH_3CO]^+$ are 53.8 kcal/mol lower in enthalpy than $[Zn(L)]^{2+}$. The reverse barrier, $\Delta H_{r0}^{\ddagger}$, at 73.0 kcal/mol is large and partially reflects the Coulombic repulsion encountered in bringing the product ions from infinity to re-form the doubly charged precursor ion. Details of the other PESs are summarized in Table 4. It is evident that the reaction enthalpy exhibits a negative correlation with IE2 (Fig. 10), while the reverse barrier ($\Delta H_{r0}^{\ddagger}$, **TS2**-products) exhibits a positive correlation (not plotted). All these results show that the higher the value of IE2, the easier it is to cleave the amide bond to give $[M(NH_2)]^+$ and $[CH_3CO]^+$.

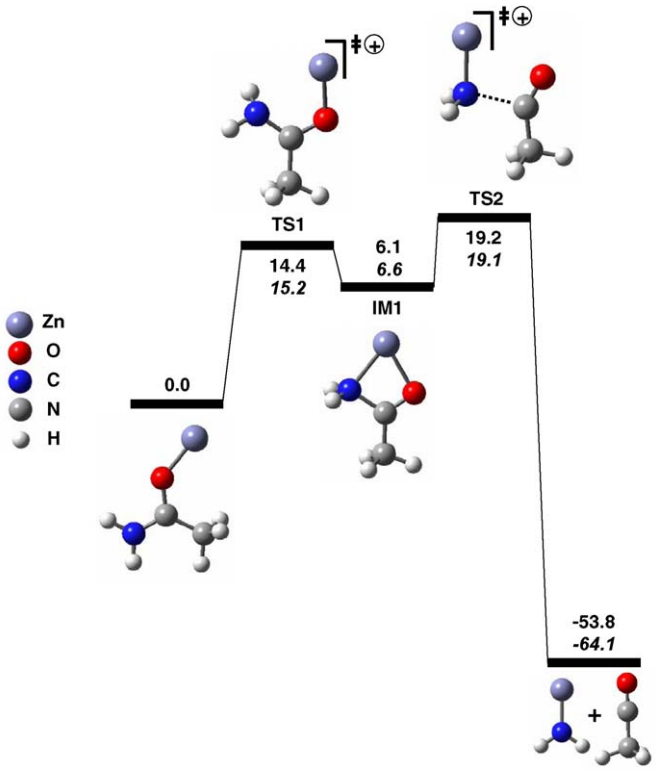

Fig. 9. Potential energy hypersurface for amide-bond cleavage in $[Zn(L)]^{2+}$: upper numbers are ΔH_0° and italicized lower number are ΔG_{298}°; both values are in kcal/mol.

Table 4
Enthalpies (in kcal/mol at 0 K) of structures on the potential energy profile for cleaving the amide bond (CO—NH_2) of ions $[M(L)]^{2+}$, where M is Ca, Mg, Zn, Ni, Cu[a]

Structure	Ca	Mg	Zn	Ni	Cu
Products, $[M(NH_2)]^+ + [CH_3CO]^+$	6.3	−16.9	−53.8	−65.4	−75.9
Intermediate **IM1** (M attached to N and O)	22.2	12.7	6.1	6.1	10.9
Transition state, **TS1**	22.5	19.8	14.4	16.9	16.1
Transition state, **TS2**	55.8	39.0	19.2	28.4	30.3

[a] Structure numbers are taken from Fig. 9 and all enthalpies are relative to $[M(L)]^{2+}$.

5.2. Dissociation of $[M(L-H)(L)]^+$ versus IE2

As alluded to earlier, increasing the orifice voltage promotes dissociation of the doubly charged $[M(L)_n]^{2+}$ complexes to give

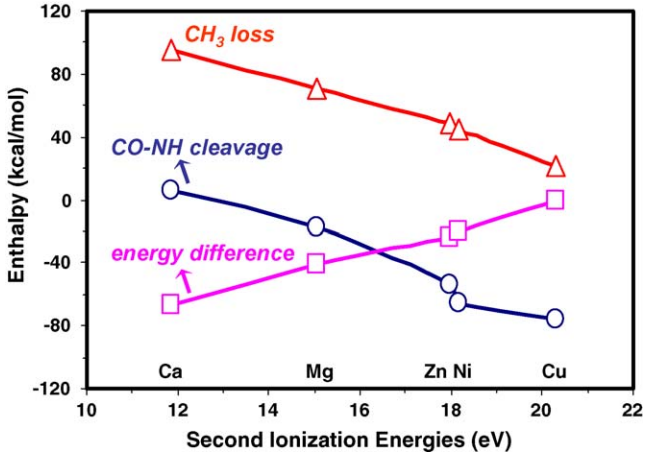

Fig. 10. Reaction enthalpy for amide-bond cleavage in $[M(L)]^{2+}$, energy difference ($\Delta\Delta H_0^{\circ}$) between losing acetamide and $(L-H)^{\bullet}$ from $[M(L-H)(L)]^+$, and reaction enthalpy for eliminating the methyl radical from $[M(L-H)]^+$ vs. IE2 for M = Ca, Mg, Zn, Ni, and Cu; all values are in kcal/mol.

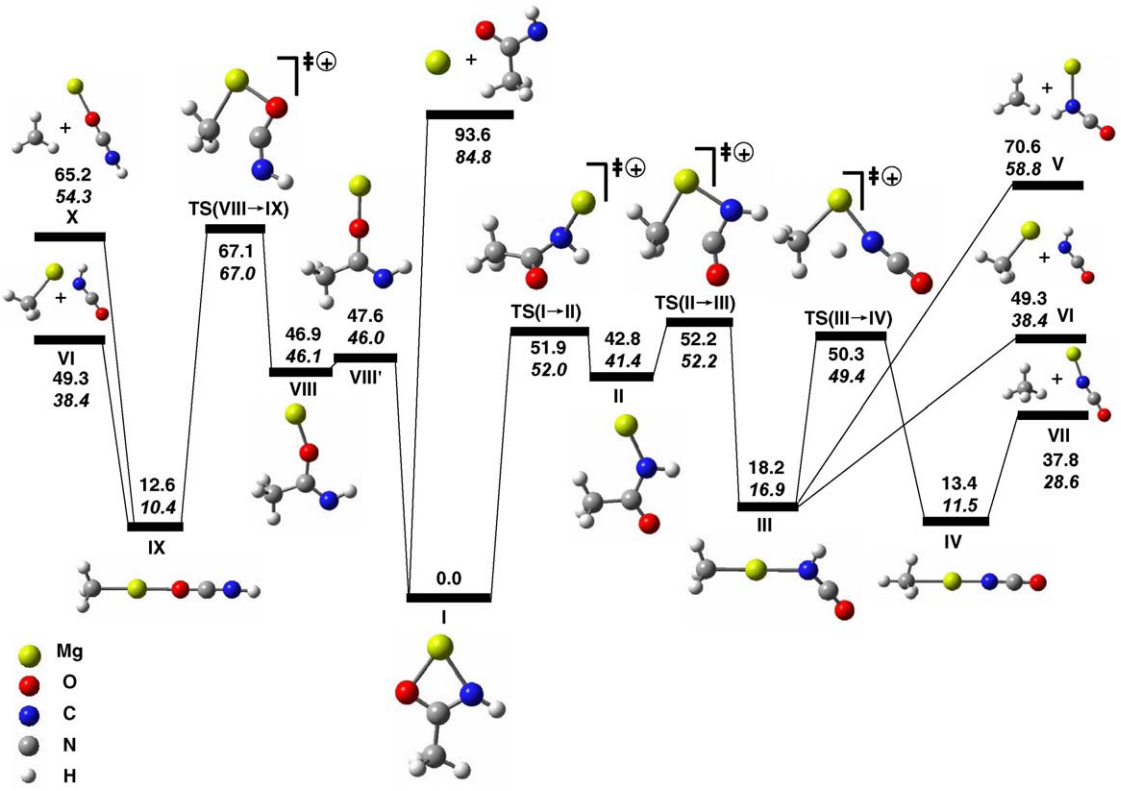

Fig. 11. Potential energy hypersurfaces for $[Mg(L-H)]^+$ dissociation: upper numbers are ΔH_0° and italicized lower number are ΔG_{298}°; both values are in kcal/mol.

$[M(L-H)(L)]^+$ and $[L+H]^+$ in the lens region by inter-ligand proton transfer. The $[M(L-H)(L)]^+$ ions dissociate by two pathways, elimination of acetamide to produce $[M(L-H)]^+$ and elimination of a neutral radical $(L-H)^\bullet$ to form $[M(L)]^+$. We have calculated the dissociation energies (ΔH_0° and ΔG_{298}°) for $[M(L-H)L]^+$ (M = Mg, Ca, Ni, Cu, Zn):

$$[M(L-H)(L)]^+ \rightarrow [M(L-H)]^+ + L \quad (5)$$

$$[M(L-H)(L)]^+ \rightarrow [M(L)]^+ + (L-H)^\bullet \quad (6)$$

Except for M = Cu, the dissociation energies for formation of $[M(L-H)]^+$ are lower than those for formation of $[M(L)]^+$. In the complex $[M(L-H)L]^+$, the ligand L is coordinated only through the oxygen, while $(L-H)$ is di-coordinated through both the oxygen and nitrogen atoms. Hence, dissociation of L occurs at lower energies.

To evaluate the extent of IE2 of the metal affects the distribution of product ions, $[M(L-H)]^+$ and $[M(L)]^+$, the energy differences ($\Delta\Delta H_0^\circ$) were calculated and are plotted against IE2 of the metals (also in Fig. 10). Interestingly, the energy difference decreases as the IE2 of the metals increases. In the complex $[M(L-H)(L)]^+$, the metal is formally M(II) and formation of $[M(L-H)]^+$ does not involve reduction of M; decomposition to $[M(L)]^+$ requires reduction from M(II) to M(I). The latter process will be energetically favored for metals with a high second ionization energy. Thus, complexes $[M(L-H)L]^+$ (except when M = Cu) fragment to produce $[M(L-H)]^+$ by loss of the neutral ligand; the copper complex is the exception because of the high IE2 of the copper.

5.3. Elimination of a methyl group or a methane molecule from $[M(L-H)]^+$ (M = Ca, Mg, Zn)

Collision-induced dissociations of the $[M(L-H)]^+$ complexes lead to cleavage of the C–O or the C–C bond. For complexes containing transition metal ions, the abundances of ions formed by cleaving the C–C bond ($[M(CH_3)]^+$ and $[M(HNCO)]^+$), relative to those formed by cleaving the C–O bond ($[M(OH)]^+$ and $[CH_3CNH]^+$) increase dramatically with the IE2 of the metal. Only for M = Ni is there evidence of cleaving the C–N bond. The calcium complex, $[Ca(L-H)]^+$ displays a different reactivity, elimination of a methane molecule to form $[Ca(NCO)]^+$. To illustrate the reaction mechanisms for the two dissociation channels involving breaking the C–C bond, the potential energy hypersurfaces of $[M(L-H)]^+$ (M = Ca, Mg, Zn) have been investigated. The PES for M = Mg is shown in Fig. 11; the enthalpies of the products and highest-energy transition states for ions containing Ca, Mg and Zn (relative to $[M(L-H)]^+$ at 0 K) are given in Table 5.

In the initial complex, structure **I**, the metal binds to both the nitrogen and to the oxygen. Rotation of the carbonyl group away from the metal ion, via **TS(I → II)**, results in isomerization to structure **II**. Stretching the C–C bond of structure **II**, leads to C–C bond cleavage and formation of M–C bond, producing structure **III**, $[M(CH_3)(HNCO)]^+$. When M is Zn, structure **III** has the lowest energy on the reaction profile. Structure **III** may eliminate a methyl radical to yield $[M(HNCO)]^{\bullet+}$ (products **V**) or lose neutral HNCO to yield $[MCH_3]^+$ (products **VI**). A third competitive pathway involves a 1,3-proton transfer from NH to

Table 5
Enthalpies (in kcal/mol at 0 K) of structures at critical points on the potential energy profile for cleaving the C—C bond of ions $[M(L-H)]^+$, where M is Ca, Mg or Zn[a]

Structure	Ca	Mg	Zn
Product **VI**, $[M(CH_3)]^+ + HNCO$	69.1	49.3	18.8
Product **VII**, $[M(NCO)]^+ + CH_4$	24.8	37.8	33.8
Product **V**, $[M(HNCO)]^{\bullet+} + CH_3^{\bullet}$	95.8	70.6	48.9
Product **X**, $[M(OCNH)]^{\bullet+} + CH_3^{\bullet}$	88.7	65.2	49.8
Intermediate **VIII** (M attached to O)	34.2	46.9	38.7
Intermediate **II** (M attached to N)	40.5	42.8	26.5
Intermediate **III**	48.2	18.2	−16.6
Intermediate **IX**	42.4	12.6	−15.6
TS(II → III)	56.0	52.2	47.0
TS(VIII → IX)	64.3	67.1	69.2
TS(III → IV)	52.4	50.3	44.6

[a] Structure numbers are taken from Fig. 11 and all enthalpies are relative to $[M(L-H]^+$.

the methyl group in structure **III** making a H_3C–H bond, and is accompanied by a significant elongation of the M–C bond, to give structure **IV**. Cleavage of the weak M–C bond in structure **IV** yields the final product **VII**, $[M(NCO)]^+$, with concomitant loss of CH_4. Alternatively, it could be the C–N bond of structure **I** that breaks resulting in structure **VIII**. Elongation of the C–C bond of structure **VIII**, via **TS(VIII → IX)**, produces structure **IX**. This ion may eliminate a methyl radical to yield $[M(OCNH)]^{\bullet+}$ (products **X**) or lose HNCO to yield $[MCH_3]^+$ (products **VI**).

On every potential energy hypersurface, the barriers to formation of structure **III** are lower than those to structure **IX**. The activation barriers ($\Delta H_0^{\ddagger}$) via **TS(VIII → IX)** are, for M = Ca, 64.3 kcal/mol; Mg, 67.1 kcal/mol; and Zn, 69.2 kcal/mol. By comparison, the barriers via **TS(II → III)** are 56.0, 52.2, and 47.0 kcal/mol, respectively. Hence, fragmentation most probably follows the pathway on the right via structure **III**.

Starting at structure **III**, the activation barriers ($\Delta H_0^{\ddagger}$) against eliminating methane are, for M = Ca, 4.2 kcal/mol; Mg, 32.1 kcal/mol; and Zn, 61.2 kcal/mol. This indicates that once structure **III** is formed, the likelihood of eliminating methane from structure **III** is Ca » Mg > Zn; experimentally, $[Ca(L-H)]^+$ is the only complex that eliminates methane. One problem with this analysis is that **TS(II → III)** is slightly higher in energy than **TS(III → IV)** (by between 2 and 4 kcal/mol) and formation of CH_4 might be expected to occur for each complex. The largest difference is when M is Ca, again the only complex that loses CH_4.

For elimination of a methyl radical, there are three possible dissociation pathways. Structure **I** may directly lose the methyl radical to produce $[(M)(HNCO)]^{\bullet+}$; or, in two-step processes, structure **I** may isomerize to either structure **III** or **IX**, and then fragment to give $[(M)(HNCO)]^{\bullet+}$ or $[(M)(OCNH)]^{\bullet+}$. The energies of the products, $CH_3^{\bullet}$ and $[M(HNCO)]^+$ are higher than those of the transition states involved in their formation, i.e., the barriers against formation of these products are determined by the overall endothermicities of the reactions. On the $[M(L-H)]^+$ surfaces, when M is Ca and Mg, the products, **V**, are 39.8 and 18.4 kcal/mol above **TS(II → III)** and experimentally no $[M(HNCO)]^{\bullet+}$ was observed; however, when M is Zn the difference is only 1.9 kcal/mol and $[Zn(HNCO)]^{\bullet+}$ was observed. In the formation of $[M(HNCO)]^{\bullet+}$ and $CH_3^{\bullet}$ from $[M(L-H)]^+$, the metal is formally reduced from M(II) to M(I); consequently, the calculated enthalpies for these endothermic reactions are inversely related to IE2, that is Ca > Mg > Zn > Ni > Cu (Fig. 10).

6. Conclusions

Doubly charged $[M(L)_n]^{2+}$ complexes, when collisionally activated, lose neutral ligands without loss of charge. As the number of ligands becomes small, charge reduction occurs either by dissociative inter-ligand proton transfer, producing $[M(L-H)(L)_{n-2}]^+$ accompanied by loss of protonated acetamide, $[L+H]^+$, or by amide-bond cleavage resulting in $[M(NH_2)(L)_{n-1}]^+$ and $[CH_3CO]^+$. Electron transfer from the ligand to the metal, resulting in formation of $[M(L)_{n-1}]^+$ and $[L]^{\bullet+}$ was only observed in the $[Cu(L)_{2,3}]^{2+}$ complexes. At higher collision energies, complexes $[M(L-H)(L)_{n-2}]^+$ (except when M is Cu) fragment to produce $[M(L-H)]^+$ by eliminating neutral ligands, or by eliminating small molecules (H_2O, CH_3CN, $H_2C{=}C{=}O$, HNCO) to yield $[M(CH_3CN)(L-H)(L)_{n-3}]^+$, $[M(OH)(L)_{n-2}]^+$, $[M(NH_2)(L)_{n-2}]^+$, and $[M(CH_3)(L)_{n-2}]^+$, respectively. These product ions further fragment to give $[M(L-H)]^+$. $[M(NH_2)(L)_{n-1}]^+$ either loses ammonia to produce $[M(L-H)(L)_{n-2}]^+$ by inter-ligand proton transfer, or loses acetamide to give $[M(NH_2)]^+$. Collision-induced dissociation of $[M(L-H)]^+$ yields two common product ions, $[M(CH_3)]^+$ and $[M(OH)]^+$ by elimination of neutral molecules, HNCO and CH_3CN, respectively. Elimination of methane from $[M(L-H)]^+$ was only observed for M = Ca, and elimination of a methyl group occurs for M = Co, Ni, and Zn. $[Cu(L-H)(L)]^{\bullet+}$ fragments either to produce $[Cu(L)]^+$ by eliminating the neutral radical $(L-H)^{\bullet}$, or by eliminating the methyl radical to form $[Cu(HNCO)(L)]^+$, which dissociates into $[Cu(L)]^+$ and HNCO.

The value of IE2, an indicator of the affinity of M^{2+} for electrons within a complex, influences the type and correlates with the extent of fragmentation chemistries that occur. Density functional theory calculations show that as IE2 of the metal increases, inter-ligand proton transfer becomes energetically more favorable than ligand loss in the CID of $[M(L)_n]^{2+}$ for small n, in accordance with experimental observations. In addition, in a second charge reduction reaction that involves cleavage of the amide bond, the dissociation enthalpy again correlates with the IE2 of the metal. The higher the IE2, the more exothermic the reaction and the lower the activation energy becomes.

For $[M(L-H)L]^+$, as IE2 increases, the difference in dissociation energies for the formation of $[M(L-H)]^+$ and $[M(L)]^+$ becomes smaller; this means producing $[M(L)]^+$ by eliminating (L − H) becomes viable. Cu has the highest IE2 of these metals and fragmentation of $[Cu(L-H)(L)]^{\bullet+}$ results in only $[Cu(L)]^+$ with concomitant elimination of $(L-H)^{\bullet}$; no $[Cu(L-H)]^{\bullet+}$ was observed.

In the CID of $[M(L-H)]^+$, $[Ca(L-H)]^+$ is unique in that it eliminates methane to form $[Ca(NCO)]^+$; other complexes where M is Co, Ni or Zn eliminate the methyl radical to produce $[M(HNCO)]^+$. Calculated activation barriers in the potential energy hypersurfaces for eliminating methane and the methyl radical from $[M(L-H)]^+$ (M = Ca, Mg, Zn) are consistent with experimental observations. The endothermicity of the methyl radical loss channel, giving the charge reduced species $[M(HNCO)]^+$, correlates well with the IE2 of the metal in the complex $[M(L-H)]^+$.

Acknowledgements

This study was supported by the Natural Sciences and Engineering Research Council (NSERC) of Canada, MDS SCIEX, and York University.

References

[1] Y. Marcus, Ion Solvation, Wiley, New York, 1985.
[2] P. Kebarle, Annu. Rev. Phys. Chem. 28 (1977) 445.
[3] R.G. Keesee, A.W. Castleman Jr., J. Phys. Chem. Ref. Data 15 (1986) 1011.
[4] P. Kebarle, in: B.E. Conway, J.O'M. Bockris (Eds.), Modern Aspects of Electrochemistry, vol. 9, Plenum Press, New York, 1974, p. 1.
[5] A.W. Castleman Jr., K.H. Bowen Jr., J. Phys. Chem. 100 (1996) 12911.
[6] A.J. Stace, J. Phys. Chem. A 106 (2002) 7993.
[7] M. Peschke, A.T. Blades, P. Kebarle, J. Phys. Chem. A. 102 (1998) 9978.
[8] M. Peschke, A.T. Blades, P. Kebarle, J. Am. Chem. Soc. 122 (2000) 10440.
[9] M. Peschke, A.T. Blades, P. Kebarle, J. Am. Chem. Soc. 122 (2000) 1492.
[10] S.E. Rodriguez-Cruz, R.A. Jockusch, E.R. Williams, J. Am. Chem. Soc. 120 (1998) 5842.
[11] S.E. Rodriguez-Cruz, R.A. Jockusch, E.R. Williams, J. Am. Chem. Soc. 121 (1999) 1986.
[12] S.E. Rodriguez-Cruz, R.A. Jockusch, E.R. Williams, J. Am. Chem. Soc. 121 (1999) 8898.
[13] R.L. Wong, E.R. Williams, Int. J. Mass Spectrom. 232 (2004) 59.
[14] G. Vitale, A.B. Valina, H. Huang, R. Amunugama, M.T. Rodgers, J. Phys. Chem. A 105 (2001) 11351.
[15] C.W. Bock, J.P. Glusker, Inorg. Chem. 32 (1993) 1242.
[16] C.W. Bock, A. Kaufman, J.P. Glusker, Inorg. Chem. 33 (1994) 419.
[17] C.W. Bock, A.K. Katz, J.P. Glusker, J. Am. Chem. Soc. 117 (1995) 3754.
[18] A.K. Katz, J.P. Glusker, S.A. Beebe, C.W. Bock, J. Am. Chem. Soc. 118 (1996) 5752.
[19] E.D. Glendening, D. Feller, J. Phys. Chem. 100 (1996) 4790.
[20] M. Pavlov, P.E.M. Siegbahn, M. Sandström, J. Phys. Chem. A 102 (1998) 219.
[21] D. Asthagiri, L.R. Pratt, M.E. Paulaitis, S.B. Rempe, J. Am. Chem. Soc. 126 (2004) 1285.
[22] K.G. Spears, F.C. Fehsenfeld, J. Chem. Phys. 56 (1972) 5698.
[23] D. Schröder, H. Schwarz, J. Phys. Chem. A 103 (1999) 7385.
[24] A. Dreuw, L.S. Cederbaum, Chem. Rev. 102 (2002) 181.
[25] A.J. Stace, Phys. Chem. Chem. Phys. 3 (2001) 1935.
[26] D.R. Lide, CRC Handbook of Chemistry and Physics, 84th ed., CRC Press, Boca Baton, FL, 2003, p. 10.
[27] V.E. Bondybey, M.K. Beyer, Int. Rev. Phys. Chem. 21 (2002) 277.
[28] I.A. Papayannopoulos, Mass Spectrom. Rev. 14 (1995) 49.
[29] A.A. Shvartsburg, K.W.M. Siu, J. Am. Chem. Soc. 123 (2001) 10071.
[30] A.A. Shvartsburg, J.G. Wilkes, J.O. Lay, K.W.M. Siu, Chem. Phys. Lett. 350 (2001) 216.
[31] T.J. Shi, G. Orlova, J.Z. Guo, D.K. Bohme, A.C. Hopkinson, K.W.M. Siu, J. Am. Chem. Soc. 126 (2004) 7975.
[32] J.A. Stone, T. Su, D. Vukumanovic, Int. J. Mass Spectrom. 216 (2002) 219.
[33] A.A. Shvartsburg, J.G. Wilkes, J. Phys. Chem. A 106 (2002) 4543.
[34] A.T. Blades, P. Jayaweera, M.G. Ikonomou, P. Kebarle, Int. J. Mass Spectrom. Ion Process. 101 (1990) 325.
[35] A.T. Blades, P. Jayaweera, M.G. Ikonomou, P. Kebarle, Int. J. Mass Spectrom. Ion Process. 102 (1990) 251.
[36] P. Jayaweera, A.T. Blades, M.G. Ikonomou, P. Kebarle, J. Am. Chem. Soc. 112 (1990) 2452.
[37] A.T. Blades, P. Jayaweera, M.G. Ikonomou, P. Kebarle, J. Chem. Phys. 92 (1990) 5900.
[38] Z.L. Cheng, K.W.M. Siu, R. Guevremont, S.S. Berman, J. Am. Soc. Mass Spectrom. 3 (1992) 281.
[39] Z.L. Cheng, K.W.M. Siu, R. Guevremont, S.S. Berman, Org. Mass Spectrom. 27 (1992) 1370.
[40] M. Kohler, J.A. Leary, J. Am. Soc. Mass Spectrom. 8 (1997) 1124.
[41] M. Kohler, J.A. Leary, Int. J. Mass Spectrom. Ion Process. 162 (1997) 17.
[42] C. Seto, J.A. Stone, Int. J. Mass Spectrom. Ion Process. 175 (1998) 263.
[43] J.A. Stone, D. Vukomanovic, Int. J. Mass Spectrom. 185/186/187 (1999) 227.
[44] J.A. Stone, D. Vukomanovic, Chem. Phys. Lett. 346 (2001) 419.
[45] U.N. Andersen, G. Bojesen, Int. J. Mass Spectrom. Ion Process. 153 (1996) 1.
[46] B.J. Hall, J.S. Brodbelt, J. Am. Soc. Mass Spectrom. 10 (1999) 402.
[47] A.A. Shvartsburg, J. Am. Chem. Soc. 124 (2002) 12343.
[48] D. Vukomanovic, J.A. Stone, Int. J. Mass Spectrom. 202 (2000) 251.
[49] B.S. Freiser, Organometallic Ion Chemistry, Kluwer Academic Publisher, Dordrecht, 1995.
[50] M.J. Frisch, G.W. Trucks, H.B. Schlegel, G.E. Scuseria, M.A. Robb, J.R. Cheeseman, V.G. Zakrzewski, J.A. Montgomery Jr., R.E. Stratmann, J.C. Burant, S. Dapprich, J.M. Millam, A.D. Daniels, K.N. Kudin, M.C. Strain, O. Farkas, J. Tomasi, V. Barone, M. Cossi, R. Cammi, B. Mennucci, C. Pomelli, C. Adamo, S. Clifford, J. Ochterski, G.A. Petersson, P.Y. Ayala, Q. Cui, K. Morokuma, P. Salvador, J.J. Dannenberg, D.K. Malick, A.D. Rabuck, K. Raghavachari, J.B. Foresman, J. Cioslowski, J.V. Ortiz, A.G. Baboul, B.B. Stefanov, G. Liu, A. Liashenko, P. Piskorz, I. Komaromi, R. Gomperts, R.L. Martin, D.J. Fox, T. Keith, M.A. Al-Laham, C.Y. Peng, A. Nanayakkara, M. Challacombe, P.M.W. Gill, B. Johnson, W. Chen, M.W. Wong, J.L. Andres, C. Gonzalez, M. Head-Gordon, E.S. Replogle, J.A. Pople, Gaussian'98, Gaussian, Inc., Pittsburgh, PA, 2001, Rev. A. 11.
[51] A.D. Becke, Phys. Rev. A 38 (1988) 3098.
[52] A.D. Becke, J. Chem. Phys. 98 (1993) 5648.
[53] C. Lee, W. Yang, R.G. Parr, Phys. Rev. B 37 (1988) 785.
[54] W.J. Hehre, R. Ditchfield, J.A. Pople, J. Chem. Phys. 56 (1972) 2257.
[55] P.C. Hariharan, J.A. Pople, Chem. Phys. Lett. 16 (1972) 217.
[56] J. Chandrasekhar, J.G. Andrade, P.v.R. Schleyer, J. Am. Chem. Soc. 103 (1981) 5609.
[57] T. Clark, J. Chandrasekhar, G.W. Spitznagel, P.v.R. Schleyer, J. Comput. Chem. 4 (1983) 294.
[58] C. Gonzalez, H.B. Schlegel, J. Chem. Phys. 90 (1989) 2154.
[59] C. Gonzalez, H.B. Schlegel, J. Phys. Chem. 94 (1990) 5523.
[60] I. Corral, O. Mó, M. Yáñez, J.-Y. Salpin, J. Tortajada, L. Radom, J. Phys. Chem. A 108 (2004) 10080.
[61] NIST Chemistry WebBook: http://webbook.nist.gov/chemistry/.
[62] M. Beyer, E.R. Williams, V.E. Bondybey, J. Am. Chem. Soc. 121 (1999) 1565.